Evolution of the electronic structure in ultrathin Bi(111) films

Lin Miao,[1] Meng-Yu Yao,[1] Wenmei Ming,[2] Fengfeng Zhu,[1] C. Q. Han,[1] Z. F. Wang,[2] D. D. Guan,[1,3] C. L. Gao,[1,3] Canhua Liu,[1,3] Feng Liu,[2] Dong Qian,[1,3,*] and Jin-Feng Jia[1,3]

[1]*Key Laboratory of Artificial Structures and Quantum Control (Ministry of Education), Department of Physics and Astronomy, Shanghai Jiao Tong University, Shanghai 200240, China*

[2]*Department of Materials Science and Engineering, University of Utah, Salt Lake City, Utah 84112, USA*

[3]*Collaborative Innovation Center of Advanced Microstructures, Nanjing 210093, China*

(Received 19 November 2014; revised manuscript received 23 April 2015; published 12 May 2015)

By combining angle-resolved photoemission spectroscopy and first-principles calculations, we systematically studied the electronic structures of ultrathin Bi(111) films ($\leqslant$5 bilayers) epitaxially grown on Bi_2Te_3. High-resolution low-energy band dispersions and Fermi surfaces of ultrathin Bi(111)/Bi_2Te_3 films as a function of thickness were experimentally determined. Our results also indicate that the electronic structures of epitaxial Bi films are strongly influenced by the substrate compared with freestanding films. The substrate effects mainly include two aspects. First, the in-plane lattice constant of Bi(111) films is compressed, which increases the bandwidth of the surface-state-like bands. Furthermore, the band dispersion near the $\bar{\Gamma}$ point is significantly modified as well. Second, there exists a strong hybridization at the Bi/Bi_2Te_3 interface, and the hybridization effects spatially extend to three Bi bilayers.

DOI: 10.1103/PhysRevB.91.205414 PACS number(s): 73.20.−r, 73.22.−f, 75.70.Tj

Bismuth (Bi) is a heavy element and its electronic structures are highly influenced by the spin-orbit coupling. Bulk Bi crystal is famous for its novel spin-split surface states caused by the large spin-orbit coupling [1–4]. Along ⟨111⟩ direction, the stable and smallest unit of Bi is the bilayer (BL) structure [1]. Theoretically, these surface states show very interesting behavior in ultrathin films [5]. In theory, ultrathin freestanding Bi(111) BLs exhibit a semiconductor to semimetal transition with the increase of thickness and the crossover thickness is 4 or 5 BLs depending on the strength of inter-bilayer coupling [5,6]. Theoretical calculations predicted that ultrathin semiconducting Bi(111) BLs were two-dimensional (2D) topological insulators (TIs) [6–8]. However, such kind of freestanding Bi(111) BLs have not been realized experimentally. It is only very recently that Bi(111) films were successfully grown on Bi_2Te_3(111) (or Bi_2Se_3) substrate from a single BL to multiple BLs [9–15], which made the experimental studies of the electronic structures of ultrathin Bi(111) films possible. Bi_2Te_3 is a 3D TI with topological Dirac-cone like surface states [16]. Recently, electronic structures of 1-BL Bi(111)/Bi_2Te_3 were studied by angle-resolved photoemission spectroscopy (ARPES) and density functional theory (DFT) calculations [9–12]. Though the band structures are very different from freestanding 1-BL Bi(111) and strong hybridization between Bi and Bi_2Te_3's surface states occurs, the nontrivial topological properties were confirmed in 1-BL Bi(111)/Bi_2Te_3 by scanning tunneling microscopy and ARPES [9,10,13,17]. However, no high-resolution band structures have been reported on multi-BL Bi(111)/Bi_2Te_3 films. It is important to know how the electronic structure changes from 1-BL to multi-BL in the Bi/Bi_2Te_3 system. It is also very interesting to know the interaction or hybridization between Bi and Bi_2Te_3 beyond single-BL Bi(111) films. By combining ARPES and DFT calculations, in this paper we studied the electronic structures of Bi(111) films ($\leqslant$5 BLs) on Bi_2Te_3 substrate. The energy bands and Fermi surface (FS) topology were experimentally determined. The effects of the substrate were discussed in detail. Surface-state-like states in Bi(111) are modified due to the stress of the Bi/Bi_2Te_3 interface. Except for single-BL Bi(111), there is no hybridization between Bi and the Dirac-cone surface states of Bi_2Te_3. Hybridization between Bi and Bi_2Te_3's bulk bands exists within 3 BLs from the interface.

Bi_2Te_3(111) films of 40 quintuple layers (QLs) were grown by MBE on a Si(111) wafer. Bi(111) films were grown on Bi_2Te_3 at 250 K. ARPES measurements were carried out with a helium discharge lamp (He-I 21.2 eV) using a Scienta analyzer and in Advanced Light Source beamlines 4.0.1 and 12.0.1. Energy resolution is better than 25 meV and angular resolution is better than 1% of the Brillouin zone (BZ). The sample temperature was kept at 100 K during measurements. DFT calculations were carried out in the framework of the generalized gradient approximation with the Perdew-Burke-Ernzerhof functional using the VASP package [18]. The in-plane lattice constant of Bi(111) films was strained to match the substrate lattice parameter. All calculations were performed with a plane-wave cutoff of 600 eV on an $11 \times 11 \times 1$ Monkhorst-pack k-point mesh. The substrate was modeled by a slab of 6-QL Bi_2Te_3, and the vacuum layers were over 20 Å thick to ensure decoupling between neighboring slabs. During structural relaxation, atoms in the lower 4-QL substrate were fixed in their respective bulk positions, and Bi BLs and the upper 2 QLs of the substrate were allowed to relax until the forces were smaller than 0.01 eV/Å.

The sharp linelike reflection high-energy electron diffraction (RHEED) pattern of Bi_2Te_3 [Fig. 1(a)] indicates a high crystalline quality and flat surface. After the Bi deposition [Figs. 1(b) and 1(c)], the linelike RHEED pattern remains. The layer-by-layer growth mode of Bi on Bi_2Te_3 was observed by RHEED intensity oscillations as reported previously [12]. The distance between two adjacent lines in the RHEED pattern is inversely proportional to the in-plane lattice constant. Figure 1(d) shows the intensity line profiles [red dotted line in

*dqian@sjtu.edu.cn

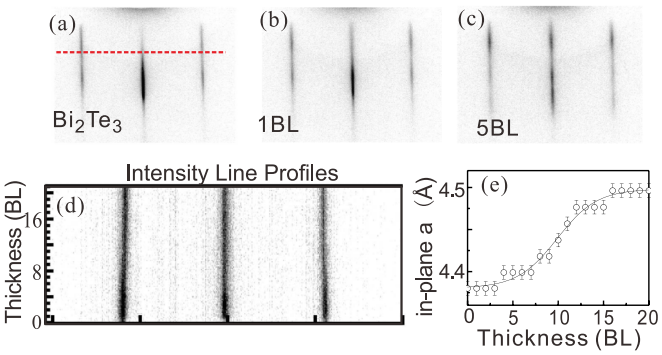

FIG. 1. (Color online) RHEED patterns of (a) 40-QL Bi_2Te_3 grown on Si(111), and (b) 1-BL Bi(111) and (c) 5-BL Bi(111) films on Bi_2Te_3. (d) RHEED intensity line profiles with the increase of film thickness. The position where the intensity line profile was taken is marked by red dashed line in (a). (e) In-plane lattice constant of Bi films as a function of film thickness. Solid line is a guide for the eye.

Fig. 1(a)] with the increase of Bi thickness. Zero BL refers to the substrate. By tracing the relative change of peak position in Fig. 1(d), we obtained the in-plane lattice constant of Bi (a_{Bi}) as a function of thickness [Fig. 1(e)]. Thinner than 3 BLs, a_{Bi} is nearly the same as the substrate (4.38 Å) within the experimental uncertainty. Then a_{Bi} increases slightly. Thicker than ~7 BLs, a_{Bi} begins to increase quickly until about 15 BLs. After 15 BLs, a_{Bi} reaches ~4.5 Å that is very close to bulk Bi (4.54 Å). Smooth change of a_{Bi} and lack of dislocations confirmed by STM indicate that strain in the films is very likely released through continuous increase of a_{Bi} in each BL.

Figure 2 presents the ARPES spectra along high-symmetry directions. Spectra of Bi_2Te_3 are shown in Fig. 2(a). Blue dotted lines mark the Dirac-cone-like surface states and valence bands of Bi_2Te_3. In Figs. 2(b)–2(k), green dotted lines are the theoretical bands. (Note that although DFT calculations were carried out with the substrate, the theoretical bands we plotted did not include the spectra of the substrate. The thickness of 1 BL is about 0.4 nm. Because the ARPES probing depth is about 1 nm, we only plotted contributions from top 2-BL Bi for 2–5 BLs Bi films to compare with experimental spectra.) According to previous calculations, freestanding Bi(111) films ($a_{Bi} = 4.54$ Å) thinner than 5 BLs are semiconductors [6] and strained freestanding Bi(111) films ($a_{Bi} = 4.38$ Å) are semiconductors below 2 BLs [13]. Experimentally, we found that the Fermi level did not locate in the energy gap for all films. There is charge transfer between the films and the substrate. The Te atoms on the Bi_2Te_3 surface would have a larger electronegativity than the Bi. This charge transfer phenomenon was confirmed by DFT calculation. In Fig. 2(l), we show the differential charge density, defined as $\Delta\rho = \rho_{Bi+Bi_2Te_3} - \rho_{Bi} - \rho_{Bi_2Te_3}$, for 3-BL Bi(111)/$Bi_2Te_3$. Substantial charge transfer at the interface occurs. $\Delta\rho$ is negative on the Bi side and positive on the Bi_2Te_3 side, which means that electrons are transferred from Bi to Bi_2Te_3.

ARPES spectra of 1-BL Bi [Fig. 2(b)] are very different from other thicknesses. The agreement between experimental spectra and DFT calculations is very good for 1-BL film. Since we have discussed 1-BL results in our previous reports [12,14], we will not discuss them in detail here. The main conclusions on 1-BL film are that there is strong hybridization between Bi and Bi_2Te_3 due to close energy proximity, which results in the appearance of Dirac-cone-like states in Bi layers [12]. No strong chemical bond exists in the Bi/Bi_2Te_3 system [11,12]. In Fig. 2(c), for 2-BL film, the calculated spectra agree with the experimental spectra very well except for some spectral features near the $\bar{\Gamma}$ point. We overlaid the bands of Bi_2Te_3 substrate from Fig. 2(a) in Fig. 2(c) (blue dotted

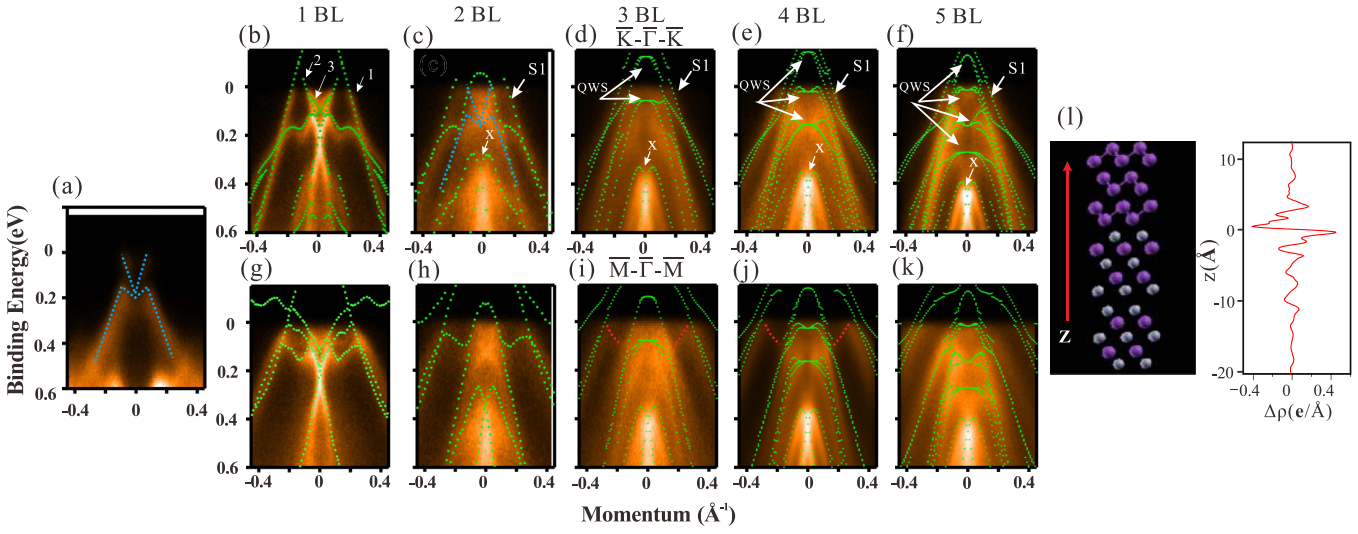

FIG. 2. (Color online) (a) ARPES spectra of 40-QL Bi_2Te_3(111) film along $\bar{K}$-$\bar{\Gamma}$-$\bar{K}$ direction. Blue dashed lines mark the surface states and valence bands. (b)–(f) ARPES spectra of 1-BL Bi(111) to 5-BL Bi(111) films along $\bar{K}$-$\bar{\Gamma}$-$\bar{K}$ directions. (g)–(k) ARPES spectra of 1-BL Bi(111) to 5-BL Bi(111) films along $\bar{M}$-$\bar{\Gamma}$-$\bar{M}$ direction. The green dashed lines are the calculated spectra from top 2 Bi BLs. White arrows in (b) and (g) mark the bands that cross the Fermi level to form Fermi surface. Blue dashed lines in (c) are from (a). Quantum well states are marked by "QWS". Outermost holelike band and Rashba-type splitting bands are marked by "S1" and "X". Red dotted lines in (i) and (j) present the hybridization bands. (l) The side view of 3-BL Bi(111) on Bi_2Te_3 and differential charge density near interface. 1 QL is 1 nm and 1 BL is 0.4 nm. $Z = 0$ is the interface.

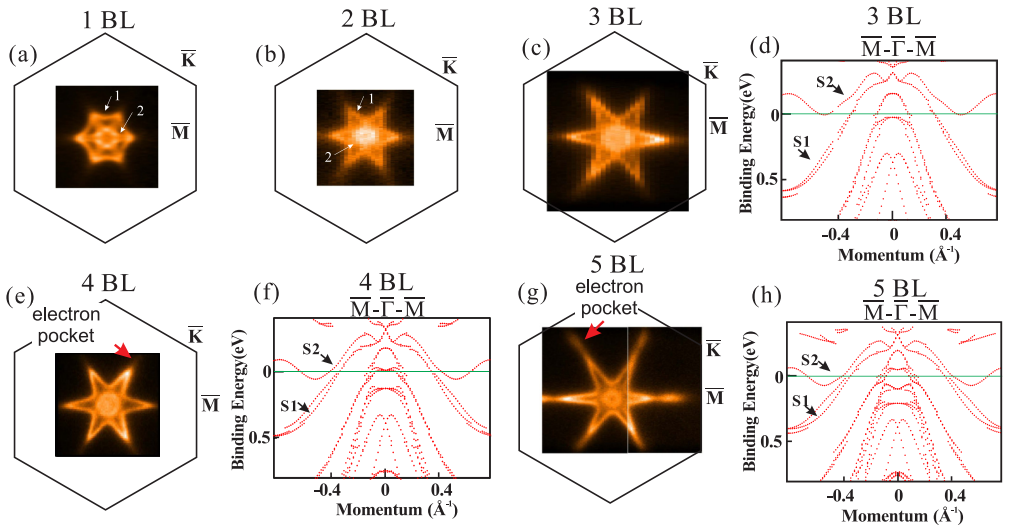

FIG. 3. (Color online) (a) Fermi surface of 1-BL and (b) 2-BL Bi(111) films. White arrows mark the outer and inner Fermi surface sheets. (c) Experimental FS and (d) the calculated bands along the $\overline{M}$-$\overline{\Gamma}$-$\overline{M}$ direction of 3-BL Bi(111)/Bi_2Te_3 film. (e) Experimental FS and (f) the calculated bands along the $\overline{M}$-$\overline{\Gamma}$-$\overline{M}$ direction of 4-BL Bi(111)/Bi_2Te_3 film. (g) Experimental FS and (h) the calculated bands along the $\overline{M}$-$\overline{\Gamma}$-$\overline{M}$ direction of 5-BL Bi(111)/Bi_2Te_3 film. Calculated bands only include the contributions from top 2-BL Bi. The Fermi levels (green lines) in calculated bands are adjusted based on the size of FS originating from S1 band.

lines). Actually, the bands from Bi_2Te_3 fit those spectra very well. For 3- to 5-BL films, no clear signals from the substrate were observed and the calculated spectra of the top 2-BL Bi are in good agreement with the experimental results along the $\overline{K}$-$\overline{\Gamma}$-$\overline{K}$ direction. There are some minor discrepancies along the $\overline{M}$-$\overline{\Gamma}$-$\overline{M}$ direction (we will discuss these later in Figs. 3 and 4). In Figs. 2(d)–2(f), two features do not change dramatically with the increase of film thickness. First, the outermost holelike bands (labeled by "S1") are similar. The S1 band has a larger Fermi vector (k_F) along $\overline{M}$-$\overline{\Gamma}$-$\overline{M}$ than along $\overline{K}$-$\overline{\Gamma}$-$\overline{K}$. According to previous calculations [5], the S1 band is "surface state" like. It is not a real surface state but will develop to a real surface state in very thick films or bulk Bi. Second, there are holelike bands with Rashba-type splitting centered at ~0.5 eV below the Fermi energy (labeled by "X"). Between the S1 band and X band, we observed more and more bands with the increase of film thickness. Consistent with previous calculations, those bands are quantum well states of Bi valence bands (labeled by "QWS") [5].

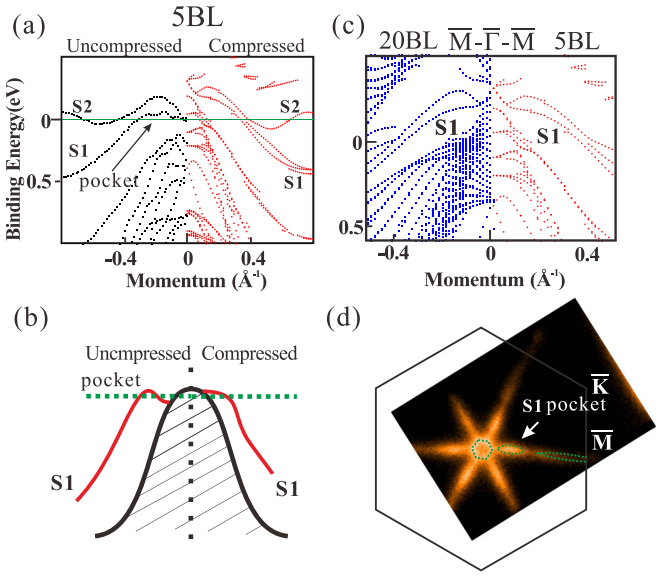

FIG. 4. (Color online) (a) Calculated band structures of 5-BL Bi(111) with uncompressed in-plane lattice constant ($a_{Bi} = 4.54$ Å) (from Ref. [5]) and of 5-BL Bi(111)/Bi_2Te_3 with compressed in-plane lattice constant ($a_{Bi} = 4.38$ Å) along the $\overline{\Gamma}$-$\overline{M}$ direction. (b) The sketch of the strain effect on S1 band. (c) Calculated band structures near $\overline{\Gamma}$ point of 20-BL and 5-BL Bi(111)/Bi_2Te_3 with compressed in-plane lattice constant ($a_{Bi} = 4.38$ Å). (d) Experimental FS of 20-BL Bi(111)/Bi_2Te_3 with ($a_{Bi} = 4.5$ Å).

Figure 3 shows the Fermi surfaces of Bi films and calculated bands along $\overline{M}$-$\overline{\Gamma}$-$\overline{M}$. Figures 3(a) and 3(b) show the measured FS of 1- and 2-BL films. The FS of the 1-BL film consists of two Fermi sheets. The outer big hexagonal sheet originates from the outermost holelike band [labeled by "1" in Fig. 2(b)]. The inner FS is a small circle with six horns along the $\overline{\Gamma}$-$\overline{M}$ direction. The inner FS is an electron pocket originating from band "2" and band "3" [labeled in Fig. 2(b)]. For the 2-BL film, the FS also consists of two sheets. Different from the 1-BL film, both sheets are hole pockets. The outer FS sheet is hexagram-like. The inner small sheet is rounded. The FS of the 3-BL film [Fig. 3(c)] shows two hole pockets, which is similar to the 2-BL film. The outer FS is related to the S1 band and the inner circle is related to QWS. According to DFT calculations [Fig. 3(d)], there are two surface-state-like bands (labeled by "S1" and "S2") near the Fermi level. In bulk Bi(111), S1 and S2 are two real surface states caused by Rashba-type spin-orbital splitting. In freestanding thin films ($a_{Bi} = 4.54$ or 4.38 Å), due to the interaction between upper and bottom surfaces, the degeneracy of the S1 and S2 bands at the $\overline{\Gamma}$ and $\overline{M}$ points is removed [5,13]. Especially, there opens a large energy gap at the $\overline{M}$ point. Differently from freestanding film, our calculations shows that the splitting between S1 and S2 bands is nearly zero at the $\overline{\Gamma}$ point for Bi/Bi_2Te_3. Usually, the calculated Fermi level is not

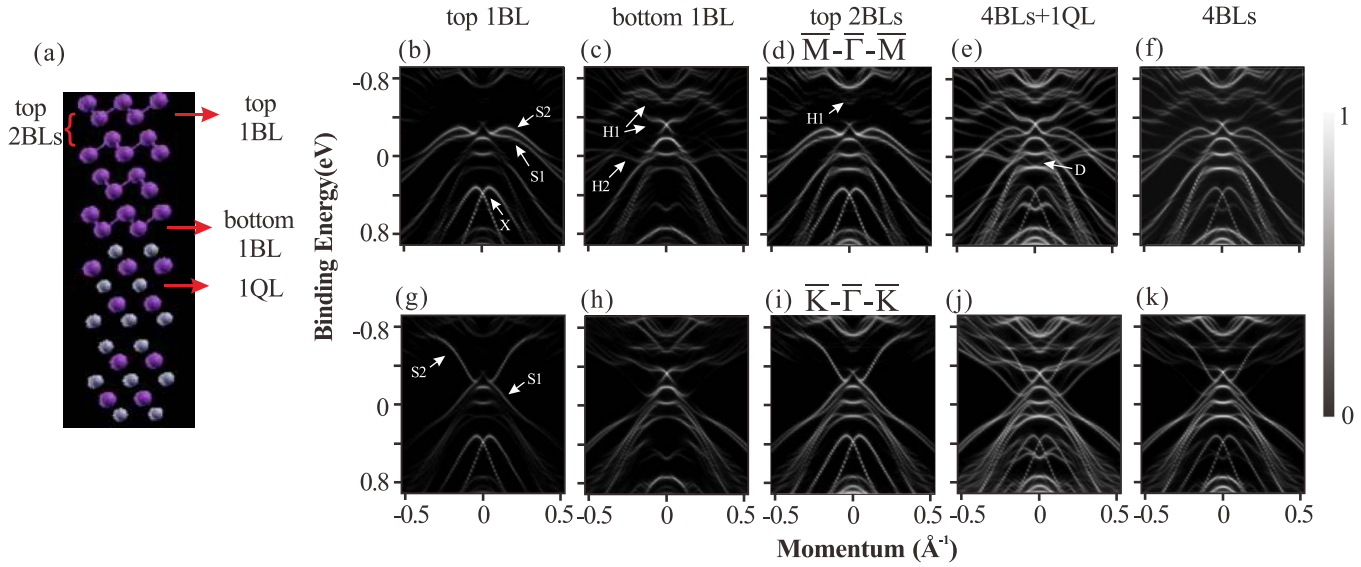

FIG. 5. (Color online) (a) Side view of 4-BL Bi(111) film on Bi_2Te_3. The calculated spectra projected onto (b) top 1 BL, (c) bottom 1 BL, (d) top 2 BLs, (e) 4 BLs plus 1-QL Bi_2Te_3(111), and (f) 4 BLs along $\overline{M}$-$\overline{\Gamma}$-$\overline{M}$ directions in 4-BL Bi(111)/Bi_2Te_3. The spectra caused by hybridization between Bi and Bi_2Te_3 are marked by "H1" and "H2" in (c). The Dirac-cone surface states of Bi_2Te_3 are marked by "D" in (e). (g)–(k) The calculated spectra projected onto the top 1 BL, bottom 1 BL, top 2 BLs, 4 BLs plus 1 QL, and 4 BLs along $\overline{K}$-$\overline{\Gamma}$-$\overline{K}$ direction.

exactly the same as experiments, so we have to adjust the Fermi level of the calculated bands to compare with experiments. Based on the experimental k_F, the determined Fermi level of 3-BL Bi (green line) cuts through the bottom of the S2 band [Fig. 3(d)], which results in a tiny electron pocket. In contrast, no electron pocket was observed along the $\overline{\Gamma}$-$\overline{M}$ direction in 3-BL film. In Figs. 3(f) and 3(h), with the increase of Bi thickness, the energy gap between the S1 and S2 bands at the $\overline{M}$ point decreases and the size of the electron pocket related to the S2 band increases. ARPES spectra show the same trend, though the observed electron pockets are smaller than calculations.

We believe that the discrepancy between experiments and calculations along the $\overline{\Gamma}$-$\overline{M}$ direction is related to a_{Bi}. In our DFT calculations, we assumed that a_{Bi} of Bi films is uniform and the same as the substrate. In real films, it is not. Each Bi BL can have different a_{Bi} that is larger than the substrate. The S1 and S2 bands are sensitive to the lattice constant. To illustrate how the in-plane lattice compression affects the S1 and S2 bands' dispersion, we compared the DFT results of uncompressed ($a_{\mathrm{Bi}} = 4.54$ Å) and compressed ($a_{\mathrm{Bi}} = 4.38$ Å) 5-BL Bi(111) in Fig. 4(a). There are two main differences between the two cases. First, the S2 band is much flatter in uncompressed film. As Fig. 4(a) shows, the electron pocket related to S2 becomes smaller when a_{Bi} is larger, which explains the discrepancy between experiments and DFT calculations along the $\overline{\Gamma}$-$\overline{M}$ direction. Second, the dispersion of the S1 band near the $\overline{\Gamma}$ point changes a lot. As illustrated in Fig. 4(b), S1 crosses E_F twice in uncompressed film and once in compressed film. This effect is thickness independent if a_{Bi} does not change. We did DFT calculations on 20-BL film with $a_{\mathrm{Bi}} = 4.38$ Å. In Fig. 4(c), S1 bands in 5-BL and 20-BL Bi(111) ($a_{\mathrm{Bi}} = 4.38$ Å) have similar dispersion relations near the $\overline{\Gamma}$ point. Experimentally, we also measured the FS of 20-BL Bi/Bi_2Te_3 ($a_{\mathrm{Bi}} = 4.5$ Å). Because of the large a_{Bi}, the measured FS is the same as bulk Bi(111) [1] [Fig. 4(d)]. S1 crosses E_F twice to form six hole pockets.

Finally, we discuss the hybridization effect between Bi and the substrate. Figure 5 shows the layer dependence of the projected spectra in DFT calculations for 4-BL Bi/Bi_2Te_3. Films of other thicknesses have similar results (except 1 BL). Figures 5(b) and 5(g) present the spectra from the top 1-BL (4th BL from the interface) Bi along the $\overline{\Gamma}$-$\overline{M}$ and $\overline{\Gamma}$-$\overline{K}$ direction, respectively. S1 and S2 have large spectral weight in the top 1 BL. In Fig. 5(b), there is a large energy gap of about 0.4 eV at the $\overline{\Gamma}$ point. In freestanding films, a similar gap exists [5]. Away from the $\overline{\Gamma}$ point, there are some weak spectra coming from QWS of the Bi conduction bands. Figures 5(c) and 5(h) present the spectra from the bottom 1-BL (1st BL from the interface) Bi. The band "X" is very strong in the top 1 BL but has no spectral weight in the bottom 1 BL. Very differently from the top 1 BL, in Fig. 5(c), strong electron-like bands (labeled by "H1") exist within the gap. In Fig. 5(h), other electron-like spectra also exist in the valence bands (labeled by "H2"). The H1 and H2 bands are caused by the hybridization between Bi and Bi_2Te_3. According to DFT, the H1 bands can extend to the third BL from the Bi/Bi_2Te_3 interface. Figure 5(d) presents the total spectra from the top 2 BLs of Bi. H1 bands already exist in the gap, though the spectral weight is weak. There is no H2 bands in the top 2 BLs. Because H1 bands are above the Fermi level, we can only detect H2 bands experimentally. In Fig. 2(j), on 4-BL Bi, we did observe spectra of weak intensity (guided by red dotted lines) from H2. In Fig. 2(k), on 5-BL Bi, no sign of the H2 bands is resolvable. Considering our ARPES depth length ($\sim$1 nm $\approx$ 3 BLs), we think H2 states should locate 2 or 3 BLs below the surface for 4-BL film as DFT suggested. By combining DFT and ARPES results, we suggest that the hybridization effects can extend spatially to the third Bi BL (H1 bands) from the interface. Figure 5(e) presents the total

spectra of 4-BL Bi and 1-QL Bi_2Te_3. Dirac-cone states of Bi_2Te_3 appear at about 0.2 eV below the Fermi level (labeled by "D"). Figure 5(f) presents the total spectra of 4-BL Bi. Obviously, no Dirac-cone states exist in Bi layers. From DFT calculations, we know the sharing of the Dirac cone only exists in 1-BL Bi film.

In summary, we experimentally determined the low-energy electronic structures of ultrathin Bi(111) films grown on Bi_2Te_3 ($\leqslant$5 BLs) with the help of DFT calculations. The Bi(111) films we studied are all metallic. The compressed in-plane lattice constant increases the bandwidth of Bi(111) films' surface-state-like bands and changes their dispersions near the $\bar{\Gamma}$ point. The strong hybridization between Bi and the Dirac-cone states in Bi_2Te_3 observed in 1-BL film previously [12] does not occur in other thicknesses. On the other hand, the hybridization between Bi and Bi_2Te_3's bulk states can extend spatially to 3 BLs from the interface.

This work is supported by the National Basic Research Program of China (Grants No. 2012CB927401, No. 2011CB922202, No. 2013CB921902, and No. 2011CB921902), NSFC (Grants No. 11274228, No. 11174199, No. 11227404, No. 11374206, No. 91421312, No. 91221302, and No. 11134008), and Shanghai Committee of Science and Technology, China (Grants No. 12JC140530 and No. 13QH1401500). C.L.G. acknowledges support from the Shu Guang project, which is supported by the Shanghai Municipal Education Commission and Shanghai Education Development Foundation. D.Q. acknowledges support from the Top-Notch Young Talents Program and the Program for Professor of Special Appointment (Eastern Scholar). D.D.G. acknowledges support from Open Research Fund Program of the State Key Laboratory of Low-Dimensional Quantum Physics (Grant No. KF201310) and Shanghai Pujiang Program (Grant No. 14PJ1404600). J.F.J. acknowledges support from the SRFDP and RGC ERG Joint Research Scheme of Hong Kong RGC and the Ministry of Education of China (Grant No. 20120073140016, M-HKU709/12). The theoretical work conducted at University of Utah is supported by the office of Basic Energy Sciences, US Department of Energy, Grant No. DE-FG02-04ER46148. We also thank the CHPC at University of Utah and NERSC for providing the computing resources. The Advanced Light Source is supported by the Director, Office of Science, Office of Basic Energy Sciences, of the US Department of Energy, under Contract No. DE-AC02-05CH11231.

[1] P. Hofmann, Prog. Surf. Sci. **81**, 191 (2006).
[2] T. Hirahara, T. Nagao, I. Matsuda, G. Bihlmayer, E. V. Chulkov, Yu. M. Koroteev, P. M. Echenique, M. Saito, and S. Hasegawa, Phys. Rev. Lett. **97**, 146803 (2006).
[3] T. Hirahara, K. Miyamoto, I. Matsuda, T. Kadono, A. Kimura, T. Nagao, G. Bihlmayer, E. V. Chulkov, S. Qiao, K. Shimada, H. Namatame, M. Taniguchi, and S. Hasegawa, Phys. Rev. B **76**, 153305 (2007).
[4] T. Nagao, J. T. Sadowski, M. Saito, S. Yaginuma, Y. Fujikawa, T. Kogure, T. Ohno, Y. Hasegawa, S. Hasegawa, and T. Sakurai, Phys. Rev. Lett. **93**, 105501 (2004).
[5] Yu. M. Koroteev, G. Bihlmayer, E. V. Chulkov, and S. Blügel, Phys. Rev. B **77**, 045428 (2008).
[6] Z. Liu, C.-X. Liu, Y.-S. Wu, W.-H. Duan, F. Liu, and J. Wu, Phys. Rev. Lett. **107**, 136805 (2011).
[7] Shuichi Murakami, Phys. Rev. Lett. **97**, 236805 (2006).
[8] M. Wada, S. Murakami, F. Freimuth, and G. Bihlmayer, Phys. Rev. B **83**, 121310 (2011).
[9] T. Hirahara, G. Bihlmayer, Y. Sakamoto, M. Yamada, H. Miyazaki, S. Kimura, S. Blügel, and S. Hasegawa, Phys. Rev. Lett. **107**, 166801 (2011).
[10] F. Yang, L. Miao, Z. F. Wang, M. Y. Yao, F. Zhu, Y. R. Song, M. X. Wang, J. P. Xu, A. V. Fedorov, Z. Sun, G. B. Zhang, C. Liu, F. Liu, D. Qian, C. L. Gao, and J. F. Jia, Phys. Rev. Lett. **109**, 016801 (2012).
[11] Z. F. Wang, M. Y. Yao, W. Ming, L. Miao, F. Zhu, C. Liu, C. L. Gao, D. Qian, J. F. Jia, and F. Liu, Nat. Commun. **4**, 1384 (2013).
[12] L. Miao, Z. F. Wang, W. Ming, M. Y. Yao, M. X. Wang, F. Yang, F. Zhu, A. V. Fedorovc, Z. Sun, C. L. Gao, C. Liu, Q. K. Xue, C. X. Liu, F. Liu, D. Qian, and J. F. Jia, Proc. Natl. Acad. Sci. USA **110**, 2758 (2013).
[13] T. Hirahara, N. Fukui, T. Shirasawa, M. Yamada, M. Aitani, H. Miyazaki, M. Matsunami, S. Kimura, T. Takahashi, S. Hasegawa, and K. Kobayashi, Phys. Rev. Lett. **109**, 227401 (2012).
[14] L. Miao, Z. F. Wang, M. Y. Yao, F. F. Zhu, J. H. Dil, C. L. Gao, C. H. Liu, F. Liu, D. Qian, and J. F. Jia, Phys. Rev. B **89**, 155116 (2014).
[15] D. D. dos Reis, L. Barreto, M. Bianchi, G. A. S. Ribeiro, E. A. Soares, W. S. Silva, V. E. de Carvalho, J. Rawle, M. Hoesch, C. Nicklin, W. P. Fernandes, J. Mi, B. B. Iversen, and P. Hofmann, Phys. Rev. B **88**, 041404(R) (2013).
[16] M. Z. Hasan and C. L. Kane, Rev. Mod. Phys. **82**, 3045 (2010).
[17] I. K. Drozdov, A. Alexandradinata, S. Jeon, S. Nadj-Perge, H. Ji, R. J. Cava, B. A. Bernevig, and Ali Yazdani, Nat. Phys. **10**, 664 (2014).
[18] G. Kresse and J. Hafner, Phys. Rev. B **47**, 558 (1993).